ORIGINAL RESEARCH

Half-sandwich ruthenium(II) complexes with N- and N,(N,O)-donor ligands: molecular, electronic structures, and computational study

J. G. Małecki

Abstract Four η^6-p-cymene ruthenium(II) complexes with 2-(2-aminophenyl)-1H-benzimidazole (BImPhNH), 2-amino-benzimidazole (BImNH), 2-aminobenzothiazole (BTzNH), and 2-(2-hydroxyphenyl)benzoxazole (HBO) ligands have been prepared and studied by IR, ^{1}H-NMR, UV–Vis spectroscopy, and X-ray crystallography; its luminescent properties were examined. The experimental studies on the complexes have been accompanied computationally by the density functional theory (DFT) calculations.

Introduction

For many years arene ruthenium complexes play important role in organometallic chemistry. The increasing interest in the chemistry of half-sandwich ruthenium(II) complexes with different ligands, mainly N-, N,O-, and P-donors, originates from numerous application of the complexes. The organometallic ruthenium(II) complexes are used in the catalytic systems for a variety organic transformations [1–3]. Even small changes in the coordination environment around the ruthenium can play a key role in altering the redox properties of the complexes, and thus complexation of

ruthenium by various ligands is very interesting and has been widely studied [4–6]. Ruthenium(II)-arene complexes display a three-legged piano-stool structure in which the metal center is octahedral and the arene ligand occupied three coordination sites. This structural feature opens the possibility to introduce in the molecule different types of ligands, and the syntheses and structural properties of the half-sandwich ruthenium(II) complexes are widely studied, especially with N,(N,O)-donors [7–12]. Furthermore, the η^6-arene ruthenium complexes are increasingly investigated due to their cytotoxicity [13, 14]. The complexes with "piano-stool" geometry with chloride and N-donor ligands often possess good aqueous solubility combined with satisfactory lipophilicity needed to cross the cell membrane. In addition, the arene ligands stabilize the ruthenium +2 oxidation state, which makes the corresponding complexes kinetically more labile when compared to those of ruthenium(III). Furthermore, the hydrogen bonding and π-stacking are important in mechanisms of biological activity and the complexes are able to present these interactions [15–17]. The benzimidazole and benzoxazole ligands are interesting due to their biological activity and the derivatives used as ligands in this work are a good representative of these derivatives. In addition, the structural and spectral characterizations of new half-sandwich ruthenium(II) complexes containing N(N,O)-donors are of great importance.

Here is presented synthesis, crystal, molecular, and electronic structures, and spectroscopy characterization of four η^6-p-cymene ruthenium(II) complexes with 2-(2-aminophenyl)-1H-benzimidazole (BImPhNH; $C_{13}H_{11}N_3$), 2-aminobenzimidazole (BImNH; $C_7H_7N_3$), 2-aminobenzothiazole (BTzNH; $C_7H_6N_2S$), and 2-(2-hydroxy-phenyl)benzoxazole (HBO; $C_{13}H_9NO_2$) ligands. The complexes are synthesized as chloride derivatives and the luminescence properties were examined. The experimental

J. G. Małecki (✉)
Department of Crystallography, Institute of Chemistry,
University of Silesia, 9th Szkolna St., 40-006 Katowice, Poland
e-mail: gmalecki@us.edu.pl

studies on the complexes have been completed theoretical calculations by the density functional theory (DFT). Currently, DFT is commonly used to examine the electronic structure of transition metal complexes. It meets with the requirements of being accurate, easy to use and fast enough to render studies of relatively large molecules of transition metal complexes possible. DFT and time-dependent density functional theory (TD-DFT) calculations were performed to establish nature of the orbitals involved in transition processes and to correlate the structural parameters with the spectroscopic properties of the complexes. The calculated density of states showed the interactions between N(O,S)-heteroaromatic compounds with ruthenium(II) and allow to compare the strength of the ligands. Thus, the studies of electronic structures of complexes are an important area of chemistry. The basic researches reported in this article combine interest in ruthenium complexes and half-sandwich coordination compounds with N(O)-donors [18–23].

Experimental

All the reagents were commercially available and were used without further purification.

Synthesis of the complexes

A mixture of [(p-cymene)RuCl$_2$]$_2$ (0.31 g; 5×10^{-4} mol) and 2-(2-aminophenyl)-1H-benzimidazole (BImPhNH), 2-aminobenzimidazole (BImNH), 2-aminobenzothiazole (BTzNH), and 2-(2-hydroxyphenyl)benzoxazole (HBO) (1×10^{-3} mol) in methanol (50 cm^{-3}) was refluxed for 2 h, cooled and filtered. Crystals suitable for X-ray crystal analysis were obtained by slow evaporation of the filtrate.

Complex 1: [[(p-cymene)RuCl(BImPhNH)]Cl·(CH$_3$)$_2$ CO, yield 87%. IR (KBr): 3436 (v_{NH}), 3178 ($v_{CH/PhH}$), 2967, 2838, 2752 (v_{CH}), 1706 ($v_{CO(acetone)}$), 1623 (v_{CN}), 1588 ($v_{C=C}$), 1542 (v_{ring}), 1487, 1463, 1446 ($v_{ring} + v_{C=C}$), 1358 (δ_{CH}), 1221 ($\delta_{p\text{-cymene}}$), 1134 (δ_{CH}), 874 (γ_{CH}), 763 ($\gamma_{BImPhNH}$), 533 (v_{Ru-N}). UV–Vis (methanol, λ [nm] (logε)): 426.6 (1.27), 356.0 (1.38), 305.8 (2.36), 237.0 (sh), 212.0 (4.87). ^{1}H-NMR: (CDCl$_3$, ppm): 14.61 (NH$_{(imidazole)}$), 9.14 (NH$_2$), 8.24 (H13), 7.78 (H3), 7.70 (H6), 7.26 (H4/5), 7.08, 5.61, 5.46 (p-cymene), 3.03 (t, CH$_{p\text{-cymene}}$), 2.18 (acetone, p-cymene), 1.69 (p-cymene), 0.93 (p-cymene).

Complex 2: [(p-cymene)RuCl$_2$(BImNH)], yield 82%. IR (KBr): 3369 (v_{NH}), 3292 (v_{PhH}), 2965, 2923, 2872 (v_{CH}), 1631 (v_{NH}), 1594 (v_{CN}), 1560 ($v_{C=C}$), 1465 ($v_{ring} + v_{CH}$), 1383 (δ_{CH}), 1270 ($v_{ring(benzimidazole)}$), 1056 (δ_{CH}), 875 (γ_{CH}), 744, 626 (γ_{CH}). UV–Vis (methanol, λ [nm] (logε)): 458.0 (1.02), 422.0 (1.16), 313.0 (1.98), 277.2 (2.76), 214.2 (4.22). ^{1}H-NMR: (CDCl$_3$, ppm): 9.27 (NH$_{imidazole}$), 6.18 (NH$_2$), 6.86 (H14, H15), 7.14 (H13, H16), 7.55, 7.02, 6.32, 6.17, 5.61, 3.03, 2.19, 1.92, 1.58, 1.33 (p-cymene).

Complex 3: [(p-cymene)RuCl$_2$(BTzNH)], yield 89%. IR (KBr): 3437 (v_{NH}), 3298, 3219, 3130 (v_{PhH}), 2965, 2923, 2864 (v_{CH}), 1611 ($v_{NH} + v_{ring\ (thiazole)}$), 1585 ($v_{CN}$), 1565 ($v_{C=C}$), 1452 ($v_{ring} + v_{CH}$), 1382, 1342 ($\delta_{CH}$), 1275 ($v_{ring}$), 1237 ($\delta_{C-C}$), 1058, 1024 ($\delta_{CH}$), 868 ($\gamma_{CH}$), 759 ($\gamma_{Ar-H}$), 528 (($\gamma_{p\text{-cymene}}$). UV–Vis (methanol, λ [nm] (logε)): 470.0 (1.23), 336.5 (2.08), 240.2 (sh), 211.0 (4.32). ^{1}H-NMR: (CDCl$_3$, ppm): 7.60 (H14), 7.52 (H16), 7.28 (H13), 7.10 (H15), 5.50 (NH$_2$), 7.41, 7.02, 6.32, 6.17, 5.35, 2.95, 2.18, 1.60, 1.31, 1.29 (p-cymene).

Complex 4: [(p-cymene)RuCl(HBO)], yield 83%. IR (KBr): 3033 (v_{PhH}), 2963, 2872 (v_{CH}), 1613 ($v_{ring\ (oxazole)}$), 1600 (v_{CN}), 1556 ($v_{C=C}$), 1459, 1430 ($v_{ring} + v_{CH}$), 1328 (δ_{CH}), 1257 (v_{C-O-C}), 1247 (δ_{C-C}), 1059 (δ_{CH}), 878 (γ_{CH}), 763, 741 (γ_{Ar-H}), 532 ($\gamma_{p\text{-cymene}}$). UV–Vis (methanol, λ [nm] (logε)): 464.5 (1.11), 410.0 (1.24), 378.5 (2.18), 293.0 (2.57), 250.0 (sh), 230.0 (3.88), 210.5 (4.47). ^{1}H-NMR: (CDCl$_3$, ppm): 7.76 (H19), 7.56 (H16), 7.44 (H13), 7.39 (H14), 7.36 (H15), 7.13 (H22), 7.10 (H21), 6.59 (H20), 7.41, 7.02, 6.32, 6.17, 5.57, 5.50, 5.36, 2.75, 2.30, 2.18, 1.67, 1.31, 1.29, 1.11 (p-cymene).

Physical measurements

Infrared spectra were recorded on a Perkin Elmer FT-IR spectrophotometer in the spectral range 4000–450 cm^{-1} using KBr pellets. Electronic spectra were measured on a Lab Alliance UV–Vis 8500 spectrophotometer in the range of 600–180 nm in methanol solution. ^{1}H-NMR spectra were obtained at room temperature in CDCl$_3$ using a Bruker 400 spectrometer. Luminescence measurements were made in methanol solutions on an F-2500 FL spectrophotometer at room temperature.

DFT calculations

The calculations were carried out using the Gaussian09 [24] program. The DFT/B3LYP [25, 26] method was used for the geometry optimization and electronic structure determination, and electronic spectra were calculated by the TD-DFT [27] method with the use of B3LYP and CAM-B3LYP functional [28]. The calculations were performed using the DZVP basis set [29] with f functions with exponents 1.94722036 and 0.748930908 on ruthenium, and polarization functions for all other atoms: 6-31g(2d,p)-chlorine, 6-31g**-carbon, nitrogen, sulfur, and 6-31g-hydrogen. The Polarizable Continuum Model (PCM) solvent model was used in the Gaussian calculations with methanol as the solvent. The theoretical values of the isotropic shieldings were obtained by means of

computational Gauge-Independent Atomic Orbital (GIAO)/ B3LYP/6-311G** routes. GaussSum 2.2 [30] was used to calculate group contributions to the molecular orbitals and to prepare the partial density of states (PDOS) and overlap population density of states (OPDOS) spectra. The contribution of a group to a molecular orbital was calculated using Mulliken population analysis. The PDOS and OPDOS spectra were created by convoluting the molecular orbital information with Gaussian curves of unit height and FWHM of 0.3 eV. Mayer bond orders were calculated with use of QMForge program [31].

The bonding interactions between the *p*-cymene rings and heteroaromatic ligands with ruthenium complex fragments have been analyzed by means of the energy decomposition analysis implemented in ADF package, which is based on the EDA method of Morokuma and the extended transition state (ETS) partitioning scheme developed by Ziegler and Rauk. The overall bond energy ΔE can be determined from interaction energy (ΔE_{int}) and the fragment preparation energy ΔE_{prep}, the instantaneous ΔE_{int} between the two fragments can be divided into three main components: $\Delta E_{int} = \Delta E_{Pauli} + \Delta E_{elstat} + \Delta E_{orb}$. ΔE_{elstat} is the electrostatic component, calculated by superposition of the unperturbed fragment densities of the molecular geometry, corresponding to the classical electrostatic effects due to the attractive and repulsive forces; ΔE_{Pauli} represents the repulsive interactions between the fragments because two electrons with the same spin cannot occupy the same region in the space; and ΔE_{orb} is the stabilizing orbital interaction term. The calculations were performed using the Amsterdam Density Functional (ADF 2008.01) program [32] with use of the generalized gradient approximation (GGA) method with non-local exchange and correlation corrections within the PW91 functional proposed by Perdew–Wang [33, 34]. The basis sets had triple ζ quality augmented with a single set of polarization functions (*f* for the metals, *d* for the main group elements, and *p* for hydrogen) (TZP). The core electrons were left unfrozen in all the calculations. The calculations were performed on the geometries optimized in Gaussian.

Crystal structures determination and refinement

Red crystals of [(C_6H_6)RuCl(BImPhNH)]Cl·(CH_3)$_2$CO (**1**), [(*p*-cymene)RuCl$_2$(BImNH)] (**2**), [(*p*-cymene)RuCl$_2$(BTz NH)] (**3**), and [(*p*-cymene)RuCl(HBO)] (**4**) were mounted in turn on an Xcalibur, Atlas, Gemini ultra Oxford Diffraction automatic diffractometer equipped with a CCD detector, and used for data collection. X-ray intensity data were collected with graphite monochromated Mo K_α radiation ($\lambda = 0.71073$ Å) at temperature 295.0(2) K, with ω scan mode. Ewald sphere reflections were collected up to $2\theta = 50.10°$. The unit cell parameters were determined

from least-squares refinement of the setting angles of 4946, 2823, 19067, and 3681 strongest reflections. Details concerning crystal data and refinement are gathered in Table 1. During the data reduction, the decay correction coefficients were taken into account. Lorentz, polarization, and numerical absorption corrections were applied. The structures were solved by the direct method. All the non-hydrogen atoms were refined anisotropically using full-matrix, least-squares technique on F^2. The Olex2 [35] and SHELXS97, SHELXL97 [36] programs were used for all the calculations. Atomic scattering factors were those incorporated in the computer programs.

Results and discussion

The half-sandwich complexes were obtained by the reaction of [(*p*-cymene)RuCl$_2$]$_2$ with 2-(2-aminophenyl)-1*H*-benzimidazole (BImPhNH), 2-aminobenzimidazole (BImNH), 2-aminobenzothiazole (BTzNH), and 2-(2-hydroxyphenyl) benzoxazole (HBO) in methanol solutions. The 2-aminophenyl- and 2-hydroxyphenyl-ligands coordinate as bidentate ligands and the 2-aminobenzimidazole, 2-aminobenzothiazole are monodentate ones.

In the IR spectrum of the complexes the ring C=C and C=N stretching modes of the ligands are present at the wavenumber range from 1623 to 1560 cm^{-1}. The stretching modes of the NH$_2$ are observed at 3436 (**1**, **2**), 3363 cm^{-1} (**3**) and above 1600 cm^{-1}. The methyl groups of *p*-cymene ligands C–H bend modes have maxim close to 1150 cm^{-1}. The twist modes of aryl C–H are close to 870 cm^{-1}.

In the ^{1}H-NMR spectra of the complexes, the protons of *p*-cymene present set of signals characteristic for the ligand given in "Experimental" section. The NH$_2$ protons of the ligands appear at 9.14 ppm in (**1**), 6.18 ppm in (**2**), and 5.50 ppm in (**3**). The imidazole NH protons gave signals at 14.61 and 9.27 ppm for complexes (**1**) and (**2**), respectively. In addition, the signals of ligands protons have been assigned to the corresponding protons which are consistent with the numbering introduced for the molecular structures presented in Fig. 1. These assignments were based on NMR spectra calculated in the GIAO method at the B3LYP functional level of theory.

Crystal structures

The complexes (**1**) and (**4**) crystallize in the monoclinic space groups $P2_1/c$, $P2_1/n$ and the complexes (**2**) and (**3**) in orthorhombic $Pna2_1$ and $P2_12_12_1$ space groups, respectively. The molecular structures of the complexes are shown in Fig. 1. Selected bond lengths and angles are listed in Table 2. The complexes adopt a distorted piano-stool type of

Table 1 Crystal data and structure refinement details of [(*p*-cymene)Ru(BIm-PhNH)]Cl·(CH$_3$)$_2$CO (**1**), [(*p*-cymene)RuCl$_2$(BImNH)] (**2**), [(*p*-cymene)RuCl$_2$(BTzNH)] (**3**), and [(*p*-cymene)RuCl(HBO)] (**4**)

	1	2	3	4
Empirical formula	C$_{23}$H$_{25}$ClN$_3$Ru,C$_3$H$_6$O,Cl	C$_{17}$H$_{21}$Cl$_2$N$_3$Ru	C$_{17}$H$_{20}$Cl$_2$N$_2$RuS	C$_{23}$H$_{22}$ClNO$_2$Ru
Formula weight	573.51	439.34	456.38	480.94
Temperature (K)	295.0(2)	295.0(2)	295.0(2)	295.0(2)
Crystal system	Monoclinic	Orthorhombic	Orthorhombic	Monoclinic
Space group	*P*2$_1$/*c*	*Pna*2$_1$	*P*2$_1$2$_1$2$_1$	*P*2$_1$/*n*
Unit cell dimensions				
a (Å)	9.7710(3)	7.1806(5)	8.3547(2)	13.2871(15)
b (Å)	13.0322(5)	18.1386(13)	13.4758(3)	7.7975(8)
c (Å)	20.4031(7)	13.6855(10)	15.7496(4)	19.037(2)
β	97.309(3)	90	90	95.896(10)
Volume (Å^3)	2576.97(15)	1782.5(2)	1773.19(8)	1961.9(4)
Z	4	4	4	4
Calculated density (mg/m^3)	1.478	1.637	1.710	1.628
Absorption coefficient (mm^{-1})	0.839	1.181	1.303	0.954
F(000)	1176	888	920	976
Crystal dimensions (mm)	0.28 × 0.11 × 0.08	0.10 × 0.06 × 0.05	0.31 × 0.16 × 0.11	0.12 × 0.08 × 0.03
θ range for data collection (°)	3.40–25.05	3.40–25.03	3.56–25.04	3.63–25.04
Index ranges	$-11 \leq h \leq 11$	$-6 \leq h \leq 8$	$-9 \leq h \leq 9$	$-15 \leq h \leq 12$
	$-11 \leq k \leq 15$	$-21 \leq k \leq 20$	$-16 \leq k \leq 16$	$-9 \leq k \leq 9$
	$-23 \leq l \leq 24$	$-16 \leq l \leq 13$	$-18 \leq l \leq 18$	$-18 \leq l \leq 22$
Reflections collected	10,973	4,754	26,594	7,280
Independent reflections	4,558 [R_{int} = 0.0277]	2,474 [R_{int} = 0.0679]	3,123 [R_{int} = 0.0333]	3,473 [R_{int} = 0.0659]
Data/restraints/parameters	4,558/0/303	2,474/1/211	3,123/0/211	3,473/0/256
Goodness-of-fit on F^2	1.032	0.998	1.084	1.084
Final *R* indices	R_1 = 0.0315	R_1 = 0.0503	R_1 = 0.0160	R_1 = 0.0613
[$I > 2\sigma(I)$]	wR_2 = 0.0669	wR_2 = 0.1184	wR_2 = 0.0387	wR_2 = 0.1048
R indices (all data)	R_1 = 0.0455	R_1 = 0.0802	R_1 = 0.0173	R_1 = 0.1009
	wR_2 = 0.0713	wR_2 = 0.1286	wR_2 = 0.0393	wR_2 = 0.1165
Largest diff. peak and hole	0.384 and −0.266	0.740 and −1.159	0.187 and −0.384	0.994 and −0.635

structure with the ruthenium atom π-bonded to the *p*-cymene ring with an average Ru–C distance of 2.2 Å, while the distances between the ruthenium atom and the centroid of the *p*-cymene ring fall in the 1.679 Å (**1**)–1.660 Å (**3**) range similar to those observed for *p*-cymene ruthenium complexes. The ruthenium atom is also directly coordinated to both nitrogen atoms of the BImPhNH ligand, one imidazole and thiazole nitrogen atom of BImNH and BTzNH ligands and nitrogen and oxygen donor atoms of 2-(2-hydroxyphenyl)benzoxazole with a normal distance. The Ru–Cl bonds length are also normal and comparable with other ruthenium(II) half-sandwich complexes. The angles between the nitrogen heteroaromatic ligands and chlorine ligands in the complexes are close to those observed in the ruthenium(II) arene compounds. In the structures of the complexes (**1**), (**2**) and (**3**), inter- and intramolecular weak hydrogen bonds exist and these are [37, 38] collected in Table 3. In the crystal structure of complex (**4**) no classical

hydrogen bonds are presented but the short contacts between chloride, *p*-cymene, and benzoxazole ligands assemble a two-dimensional network shown in the Fig. 2.

Geometry and electronic structure

To gain insight into the electronic structures and bonding properties of these complexes, DFT calculations were carried out. Before the calculations of electronic structures of the complexes, their geometries were optimized in singlet states using the B3LYP functional. From the data collected in Table 2, one may see that the bond lengths are maximally elongated by ~0.1 Å in the calculated gas phase structures, while the change of bond angles do not outrun 8°. Figure 3 shows that the calculated and experimental IR spectra of complexes (**3**) and (**4**) are in good agreement.

The formal charge of ruthenium is +2 in all complexes. In the complex (**4**) the same charge of ruthenium central
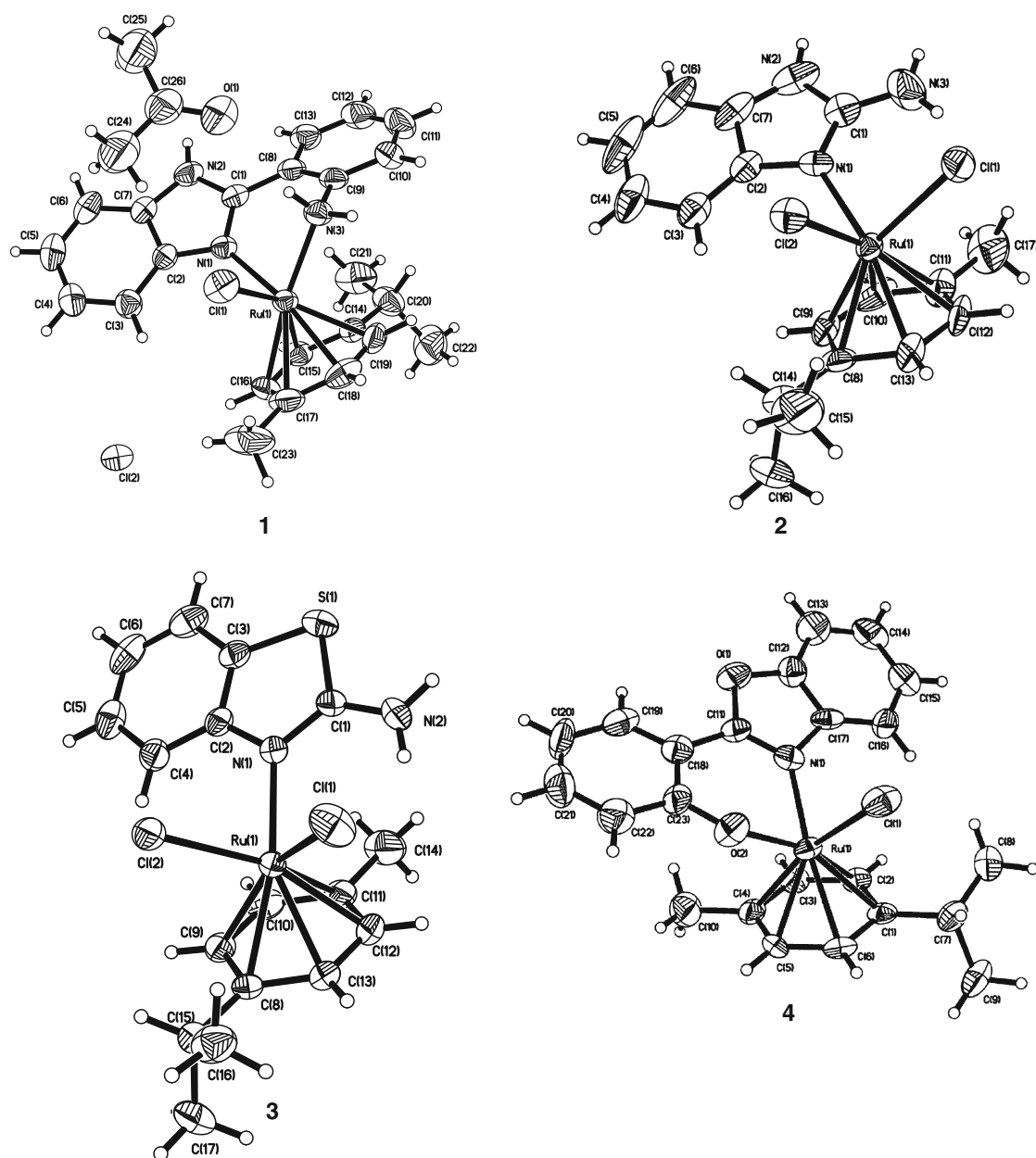
Fig. 1 ORTEP drawing of [(*p*-cymene)Ru(BIm-PhNH)]Cl·(CH₃)₂CO (**1**), [(*p*-cymene)RuCl₂(BImNH)] (**2**), [(*p*-cymene)RuCl₂(BTzNH)] (**3**), and [(*p*-cymene)RuCl(BzO)] (**4**) with 50% probability displacement ellipsoids

ion is due to the deprotonation of the hydroxyl part of the ligand during the complexation reaction. The calculated charges on the ruthenium atoms, obtained from natural population analysis, vary from 0.4 in complex (**4**) to 0.18 in complex (**3**). The charge on the chlorine ligands is equal to −0.4 and those on the nitrogen donor atoms of the ligands are about −0.5. The low charges on the Ru central ions are the results of charge donations from the ligands to the metal. The conclusion is confirmed by the second-order perturbation analysis from NBO. The stabilization energy

calculated in this analysis shows that the lone pairs localized nitrogen atoms of the BImPhNH, BImNH, BTzNH and nitrogen and oxygen HBO ligands donate the charge to the ruthenium *d* orbitals, and the stabilization energy (ΔE_{ij}) is 196.97 kcal mol⁻¹ for (**1**), 96.51 kcal mol⁻¹ for (**2**), 86.84 kcal mol⁻¹ for (**3**), and 215.83 kcal mol⁻¹ for complex (**4**), respectively. The back donation from ruthenium to the N(N,O)-donor ligands is smaller averaging to 48.26 kcal mol⁻¹ for complex (**1**), 32.47 kcal mol⁻¹ for (**2**), 33.72 kcal mol⁻¹ for (**3**), and 37.89 kcal mol⁻¹ for

Table 2 Selected bond lengths (Å) and angles (°) for [(p-cymene)Ru(BIm-PhNH)]Cl (**1**), [(p-cymene)RuCl₂(BImNH)] (**2**), [(p-cymene) RuCl₂(BTzNH)] (**3**), and [(p-cymene)RuCl(HBO)] (**4**) with the optimized geometry values

	1		2		3		4	
	Exp	Calc	Exp	Calc	Exp	Calc	Exp	Calc
Bond lengths (Å)								
Ru(1)–N(1)	2.113(2)	2.148	2.133(8)	2.189	2.169(18)	2.239	2.086(5)	2.132
Ru(1)–N(3)	2.141(2)	2.194						
Ru(1)–O(2)							2.104(4)	2.075
Ru(1)–Cl(1)	2.396(8)	2.414	2.441(3)	2.471	2.420(6)	2.424	2.4048(17)	2.423
Ru(1)–Cl(2)			2.427(3)	2.425	2.427(6)	2.469		
Ru(1)–C(1)	2.222(3)	2.309	2.209(11)	2.256	2.193(2)	2.236	2.211(6)	2.207
Ru(1)–C(2)	2.153(3)	2.222	2.171(13)	2.203	2.155(2)	2.206	2.186(6)	2.290
Ru(1)–C(3)	2.174(3)	2.255	2.163(10)	2.234	2.180(2)	2.237	2.150(6)	2.262
Ru(1)–C(4)	2.223(3)	2.288	2.207(11)	2.242	2.209(2)	2.263	2.185(6)	2.205
Ru(1)–C(5)	2.198(3)	2.249	2.149(11)	2.238	2.176(2)	2.240	2.169(5)	2.274
Ru(1)–C(6)	2.171(3)	2.238	2.138(10)	2.213	2.160(2)	2.207	2.186(5)	2.234
Angles (°)								
N(1)–Ru(1)–N(3)	79.23(9)	78.90						
N(1)–Ru(1)–O(2)							82.87(18)	85.92
Cl(1)–Ru(1)–Cl(2)			84.99(10)	87.97	84.69(2)	86.89		
Cl(1)–Ru(1)–O(2)							85.44(14)	84.58
N(1)–Ru(1)–Cl(1)	86.01(6)	85.32	92.40(2)	89.80	91.23(5)	91.14	87.07(14)	86.89
N(1)–Ru(1)–Cl(2)			83.00(2)	87.03	87.16(5)	88.33		
N(3)–Ru(1)–Cl(1)	82.12(7)	79.77						
N(1)–Ru(1)–C(1)	109.99(10)	112.83	129.00(4)	123.77	157.76(8)	160.52	130.3(2)	137.04
N(1)–Ru(1)–C(3)	132.64(12)	129.91	141.90(4)	148.54	91.47(8)	94.33	90.5(2)	93.28
N(1)–Ru(1)–C(5)	169.61(11)	166.60	88.00(4)	90.44	114.35(8)	113.02	145.1(2)	141.02
N(3)–Ru(1)–C(1)	101.58(10)	101.46						
N(3)–Ru(1)–C(3)	111.14(12)	112.83						
N(3)–Ru(1)–C(5)	169.23(11)	168.25						
Cl(1)–Ru(1)–C(1)	163.95(8)	161.86	137.60(4)	139.98	110.89(6)	108.33	90.32(16)	89.31
Cl(1)–Ru(1)–C(3)	95.99(9)	95.82	84.30(3)	87.05	158.86(7)	159.40	149.10(17)	141.60
Cl(1)–Ru(1)–C(5)	108.53(9)	111.98	128.80(5)	123.20	92.41(7)	93.47	125.60(17)	132.26
Cl(2)–Ru(1)–C(1)			91.00(4)	92.51	92.48(6)	92.00		
Cl(2)–Ru(1)–C(3)			134.10(3)	138.74	116.39(7)	113.08		
Cl(2)–Ru(1)–C(5)			145.50(5)	149.36	158.39(7)	158.62		
O(2)–Ru(1)–C(1)							146.31(19)	136.24
O(2)–Ru(1)–C(3)							124.8(2)	131.30
O(2)–Ru(1)–C(5)							87.5(2)	84.34
C(1)–Ru(1)–C(3)	68.06(12)	66.58	68.70(4)	67.69	68.79(9)	67.66	68.1(2)	67.28
C(1)–Ru(1)–C(5)	67.75(11)	66.14	69.30(5)	78.74	68.51(9)	67.57	68.1(2)	66.75
C(3)–Ru(1)–C(5)	67.09(13)	65.95	65.90(5)	66.65	67.44(10)	66.12	67.9(2)	66.53

complex (**4**), respectively. The interaction between ruthenium and N(O)-donor ligands is presented on the Fig. 4b and one may see from the overlay partial density of states (OPDOS) diagram that the 2-(2-hydroxyphenyl)benzoxazole is considerably stronger ligand in comparison of BImNH and BTzNH. The Mayer bond orders of Ru–N₍Im₎

bonds are 0.85 for (**1**), 0.79 for (**2**), 0.73 for (**3**), and 0.84 (Ru–O 1.30) for (**4**) which confirm strength of HBO ligand. The Mayer bond orders are more dependent on the bases used to calculate than the Wiberg indices which are well known. Wiberg indices in this regard are less sensitive which is important when comparing the properties of

Table 3 Hydrogen bonds for [(*p*-cymene)Ru(BIm-PhNH)]Cl (**1**), [(*p*-cymene)RuCl$_2$(BImNH)] (**2**), [(*p*-cymene)RuCl$_2$(BTzNH)] (**3**), and [(*p*-cymene)RuCl(HBO)] (**4**) complexes (Å and °)

D–H···A	d(D–H)	d(H···A)	d(D···A)	<(DHA)
1				
N(2)–H(2)…Cl(2) #1	0.86	2.28	3.105(2)	161
N(3)–H(3A)…Cl(2) #2	0.90	2.29	3.189(2)	173
N(3)–H(3B)…O(1)	0.90	2.25	3.074(3)	153
C(15)–H(15)…Cl(1) #3	0.93	2.77	3.546(3)	141
C(24)–H(24)…Cl(1)	0.96	2.70	3.580(5)	152
2				
N(2)–H(2)–Cl(2) #4	0.86	2.55	3.379(9)	162
N(3)–H(3A)–Cl(1) #4	0.86	2.43	3.229(12)	155
N(3)–H(3B)–Cl(1)	0.86	2.41	3.118(12)	140
C(12)–H(12)…Cl(2) #5	0.93	2.82	3.689(11)	156
C(15)–H(15C)…Cl(2)	0.96	2.77	3.485(15)	132
3				
N(2)–H(2A)…Cl(1)	0.86	2.42	3.081(2)	134

Symmetry transformations used to generate equivalent atoms: #1: 1 + x, y, z; #2: −x,−1/2 + y, 1/2 − z; #3: −x, 1/2 + y, 1/2 − z; #4: −1/2 + x, 1/2 − y, z; #5: 1 − x,1 − y, 1/2 + z

similar compounds, but is not sufficiently sensitive to the impact of valence orbitals of central atom on the properties of bonds. The Wiberg indices for the Ru–N$_{(Im)}$ bonds are 0.49 for (**1**), (**3**), (**4**) and 0.47 for complex (**2**). In general, the bonding between ruthenium and imidazole or benzoxazole derivatives ligand have predominant Coulomb character in contrast to the effects of chloride ligands and especially *p*-cymene rings which are covalent. Figure 4a shows OPDOS diagram for cationic complex (**1**) and one may see that the π-accepting interaction between *p*-cymene ligand and ruthenium is very strong.

Figure 5 shows density of states (DOS) diagrams for complexes (**1**), (**2**), and (**4**). The DOS plot mainly presents the composition of the fragment orbitals contributing to the molecular orbitals. As one can see from Fig. 5, d_{Ru} orbitals play a significant role in the frontier Homo orbitals of the complexes. The contributions of *d* orbitals of ruthenium central ions in occupied molecular orbitals are in the range of 48–54% (Homo, Homo-1, and Homo-4) in the cationic complex (**1**) and 10–42% (Homo–Homo-3) in neutral complexes (**2**), (**3**), and (**4**). In these molecular orbitals, chloride and heteroaromatic ligands play a significant role. As one

Fig. 2 The crystals packing of complex (**4**) viewing down the *a* axis with short contact indicated by *dotted lines*
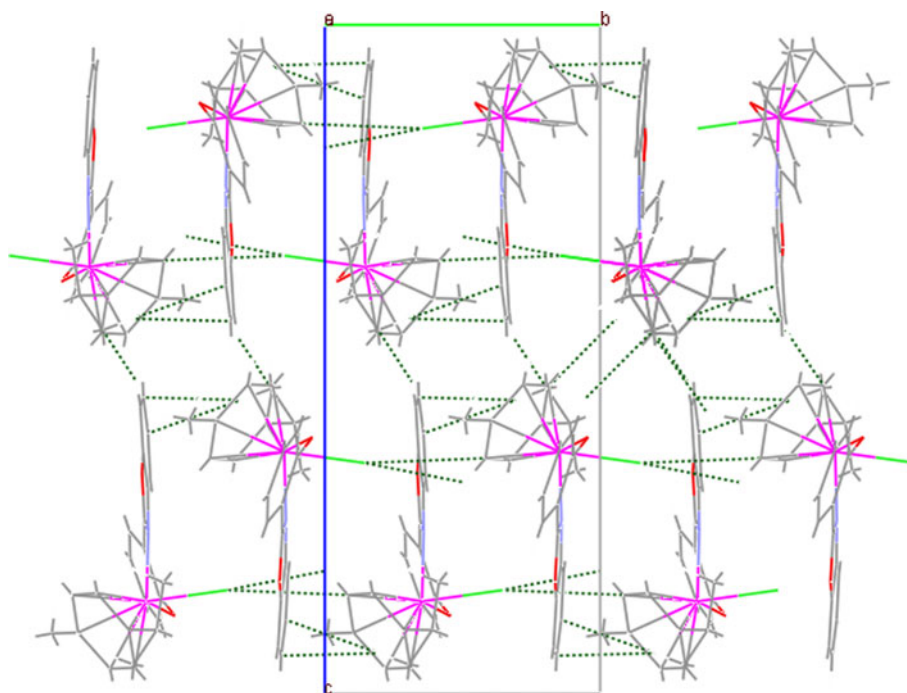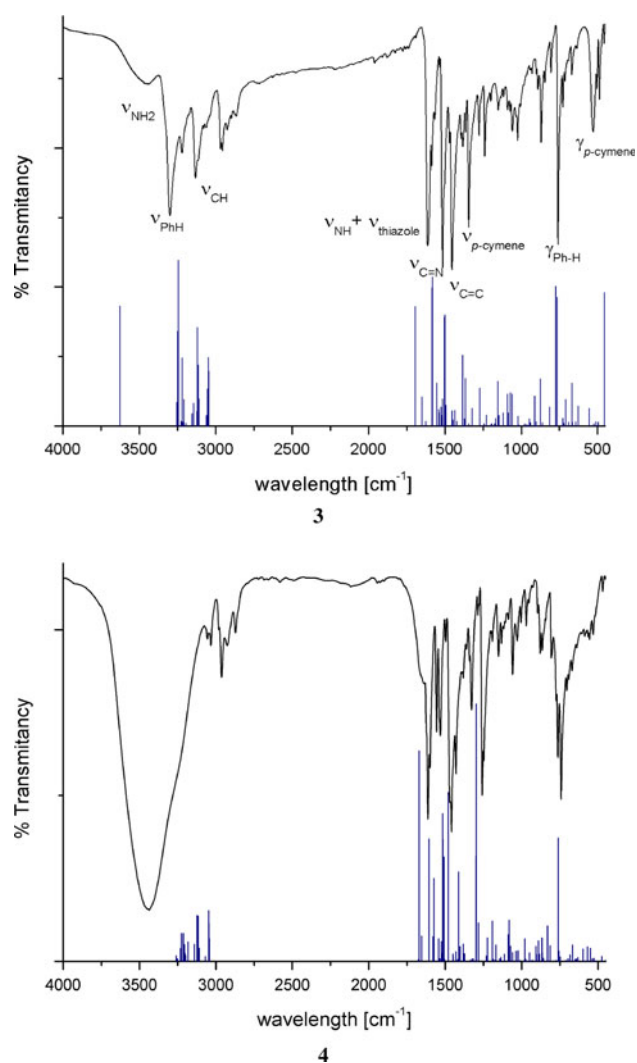
Fig. 3 The experimental and calculated IR spectra of [(*p*-cymene) RuCl₂(BTzNH)] (**3**) and [(*p*-cymene)RuCl(HBO)] (**4**) complexes
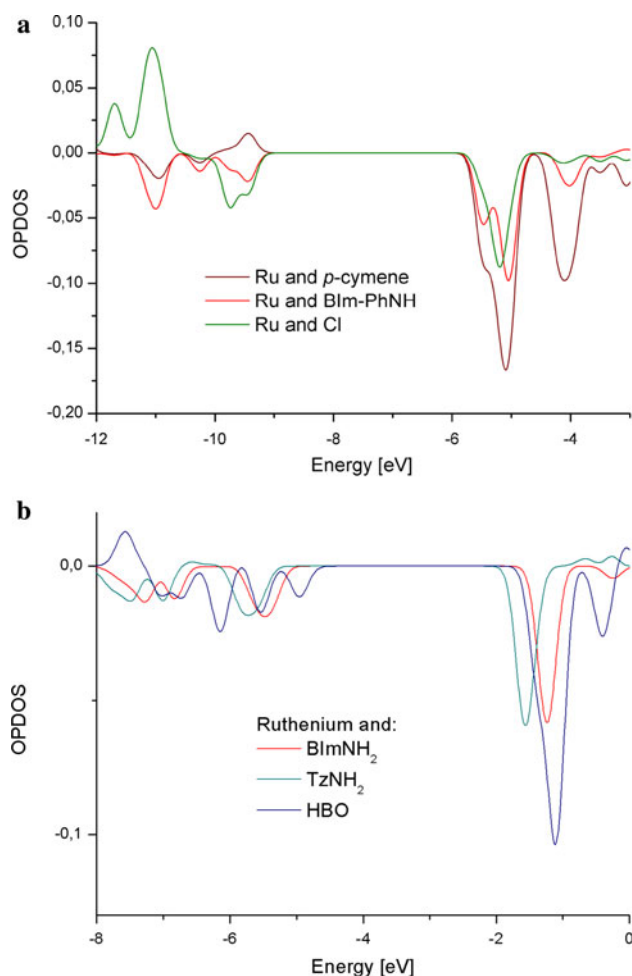

Fig. 4 The overlap partial density o states diagram for interactions of ruthenium and 2-(2-aminophenyl)-1*H*-benzimidazole (BImPhNH), 2-aminobenzimidazole (BImNH), 2-aminobenzothiazole (BTzNH), and 2-(2-hydroxyphenyl)benzoxazole (HBO) ligands

may see from the DOS diagrams, participations of bidentate ligands are meaningful larger compared to monodentate 2-aminobenzimidazole and 2-aminobenzothiazole. The frontier virtual molecular orbitals are mainly localized on the N(N,O)-donor ligands and d_{Ru} orbitals with contributions of *p*-cymene. Furthermore, d_{Ru} orbitals are diffused in energy scope corresponding to Lumo+1 to Lumo+4 (24–67%) levels. In these unoccupied orbitals, *p*-cymene and hetero-aromatic ligands play significant role.

The bonding between benzene and ruthenium is formed by the two π orbitals of e_{1g} symmetry (π_2 and π_3) and the empty *d* orbitals of the metal atom (donation from benzene to ruthenium). The resulting bonding orbitals are HOMO-12 and HOMO-15, the antibonding are LUMO and LUMO+1. In the back donation (metal to ligand) the occupied $d_{x_2-y_2}$ and d_{xz} metal orbitals and empty π_4^*, π_5^* benzene orbitals participate (HOMO-2, HOMO, and LUMO+2, LUMO+4). To

get an insight into the Ru–*p*-cymene bonds, an energy decomposition analysis has been carried out. In Table 4 are listed the result of energy decomposition analysis calculated for the complexes in methanol solvents. The repulsive interactions are dominated in the binding of arene rings with ruthenium central ions. On the other hand, the electrostatic contribution plays a role and has a stabilizing influence. In addition, the ΔE_{elstat} is slightly higher than the orbital interaction in the all complexes and the percentage contribution of the electrostatic interaction to the total attraction vary in the range of 61% in complexes (**3**) and (**4**) to 54% in complex (**1**). The data confirm the covalent character of the bonding interaction between ruthenium and *p*-cymene ring. However, when the heteroaromatic ligands are considered as fragments, the electrostatic interaction is the leading stabilization energy except the complex (**4**) in which ΔE_{Orb} plays dominant role. It drives the bonding interaction of the occupied MOs of HBO ligand with the *d* orbitals of the
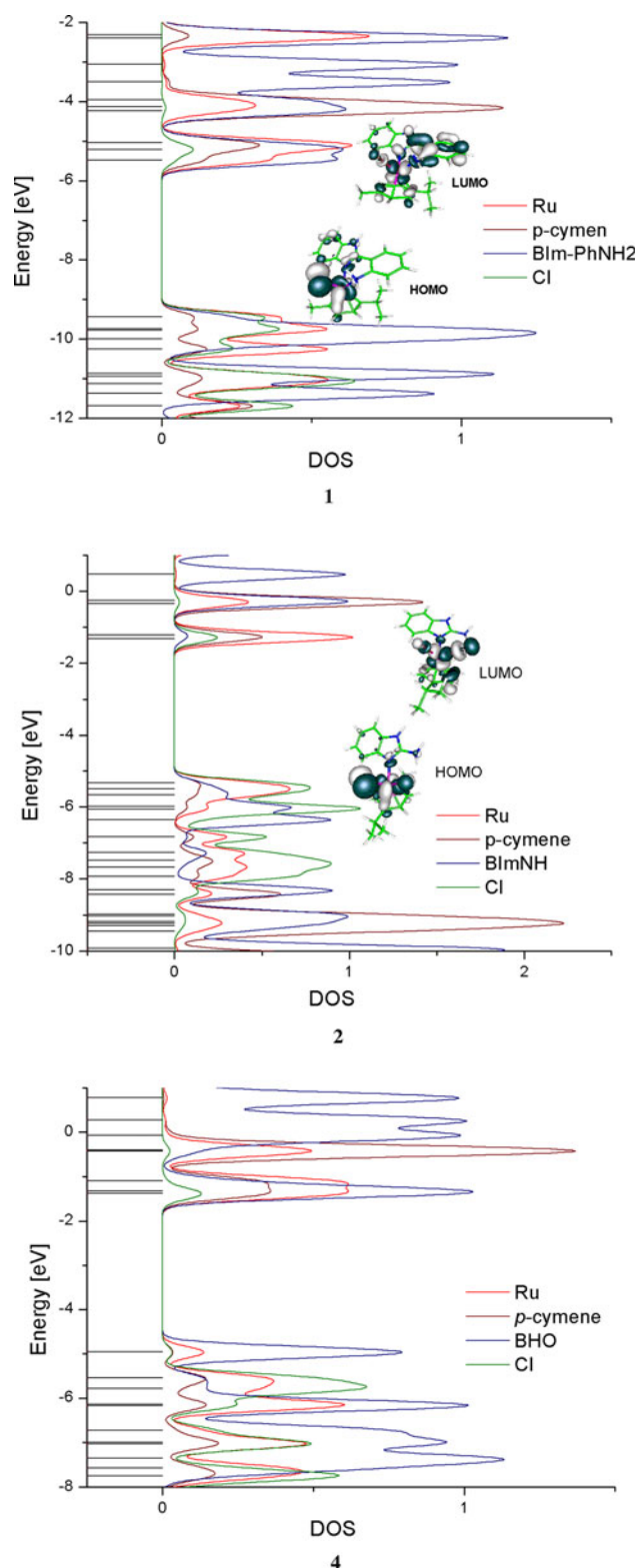
Fig. 5 The density of states (DOS) diagrams for complexes (**1**), (**2**), and (**4**)

ruthenium atom and confirms strong donor properties of HBO ligand. In addition the ΔE_{Pauli} energies are smaller than that in the *p*-cymene fragments.

Electronic spectrum

Electronic spectra of the complexes exhibit, except the intense bands connected with ligands, absorption bands originated from *d–d* transitions. The UV–Vis spectra of the complexes are similar and show bands in the ranges v_1: 427–470 nm; v_2: 410–422 nm; v_3: 313–378 nm attributed to $^1A_1 \rightarrow \, ^1A_2$, $^1A_1 \rightarrow B_1$, and $^1A_1 \rightarrow B_2$ transitions in pseudo-octahedral geometry of these complexes. Therefore, the ligand field parameters 10 Dq can be estimated to 12,140, 15,105, 15,101, and 12,766 cm^{-1} for the complexes (**1**), (**2**), (**3**), and (**4**), respectively. Racah's parameters for the complexes are B = 292, 632, 530, 305 cm^{-1}; C = 1342, 2907, 2438, 1403 cm^{-1}, respectively, and the nepheloauxetic parameters have values β_{55} = 0.41, 0.88, 0.74, and 0.42, respectively. The differences in these parameters are in accordance with the covalence of these complexes and strength of ligands interactions with ruthenium central ions.

For these complexes, the nature of the transitions observed in the UV–Vis spectra have been studied by the time-dependent density functional (TD-DFT) method based on the optimized geometries, in gas phase without any symmetry restrictions, in the singlet states. The PCM solvent model was used in the Gaussian calculations with methanol as the solvent. The experimental spectrum of complex (**4**) with the calculated transitions is presented in Fig. 6. The electronic transitions were calculated with use B3LYP and CAM-B3LYP functional. Nevertheless, the calculations with CAM-B3LYP functional showed worse results as one can see from data collected in Table 5. The assignments of the calculated transitions to the experimental bands are based on the criteria of energy and oscillator strength of the calculated transitions. In the description of the electronic transitions, only the main components of the molecular orbitals are taken into consideration.

The experimental bands in the range 470–313 nm are assigned to the transitions between the frontier HOMO and LUMO molecular orbitals. As the highest occupied and lowest virtual molecular orbitals are composed of the *d* ruthenium the transitions are of *Ligand Field* type ($d \rightarrow d$). The bands with maxima in the range 290–237 nm have *metal–ligand charge transfer* character and the highest energy bands with maxima near 212 nm are attributed to transitions of the *ligand–ligand charge transfer* type ($\pi \rightarrow \pi^*_{C=N}$).

The emission characteristics of the complexes have been examined in the methanol solutions (with concentration of 5×10^{-4} mol/dm^3) at room temperature. The excitations were executed at wavelengths corresponding to maxima of $d \rightarrow d$ character electronic absorptions, i.e., at 420 nm for (**1**) and (**2**), and 470, 460 nm for (**3**) and (**4**), respectively. The emission spectra present in Fig. 7. The fluorescence maxima

Table 4 Energy decomposition analysis for [(*p*-cymene) Ru(BIm-PhNH)]$^+$ (**1**), [(*p*-cymene)RuCl$_2$(BImNH)] (**2**), [(*p*-cymene) RuCl$_2$(BTzNH)] (**3**), and [(*p*-cymene)RuCl(HBO)] (**4**) complexes (energies in kcal mol^{-1})

Energy (kcal/mol)	1	2	3	4
[RuCl$_n$(L)] + *p*-cymene				
ΔE_{elstat}	−194.73	−238.95	−269.21	−255.93
ΔE_{Pauli}	288.43	358.32	354.13	339.19
ΔE_{orbint}	−166.55	−174.38	−179.45	−164.56
$\Delta E_{solvation}$	−58.12	−33.31	−27.53	−28.91
ΔE	−127.19	−88.32	−122.06	−106.43
[(*p*-cymene)RuCl$_n$] + L				
ΔE_{elstat}	−149.03	−92.10	−82.93	−144.34
ΔE_{Pauli}	166.46	107.58	98.38	226.31
ΔE_{orbint}	−99.42	−44.99	−42.80	−167.61
$\Delta E_{solvation}$	−54.13	−33.29	−27.35	−22.42
ΔE	−136.12	−62.81	−54.69	−108.06

are at 490, 484, 550, and 565 nm with shoulders at wavelengths shifted about 40 nm toward higher energy. As one can see from the figure, the strongest emission was detected for complex (**4**). It is associated with a substantial share of HBO ligand and d_{Ru} orbitals in frontier Homo and Lumo orbitals. Moreover, the interaction between 2-(2-hydroxyphenyl)benzoxazole and ruthenium(II) has the most covalent character among the studied complexes. Taking into account the contributions of ligand orbitals in MOs the emission originating from the lowest energy metal to ligand charge transfer (MLCT) state, derived from the excitation involving a $d_\pi \rightarrow \pi_{ligand}^*$ transition are observed. The complicated structure of the luminescence spectra suggest that more than one state is involved in luminescence processes [20].

Conclusion

From the simple reactions between [(*p*-cymene)RuCl$_2$]$_2$ and 2-(2-aminophenyl)-1*H*-benzimidazole (BImPhNH),
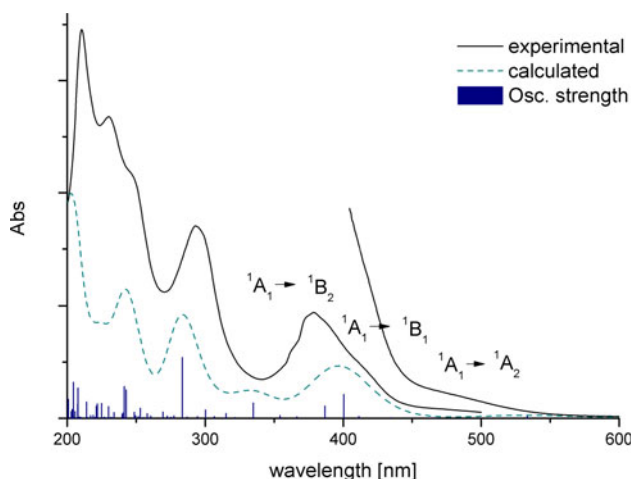

Fig. 6 The experimental and calculated UV–Vis spectra of complex (**4**) with calculated electronic transitions

2-aminobenzimidazole (BImNH), 2-aminobenzothiazole (BTzNH), 2-(2-hydroxyphenyl)benzoxazole (HBO) ligands in methanol solutions, four new half-sandwich ruthenium(II) complexes were obtained. Except the cationic complex (**1**) (with BImPhNH) the others are neutral. The molecular structures of the complexes were determined by X-ray crystallography, and the spectroscopic properties were studied.
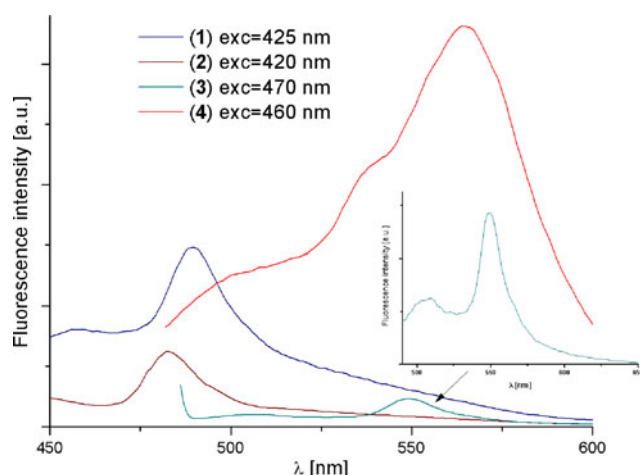
Electronic structures of the studied complexes were calculated using DFT method, and apart from the descriptions of frontier molecular orbitals the bonding properties in the complexes were determined. Based on calculated stabilizations energies, the values of the interaction between ruthenium(II) ions and heteroaromatic ligands and the energy decomposition analysis indicated the HBO was strong ligand. The differences in acceptor properties of the ligands were shown in the values of ligand field parameters determined from electronic spectra of the complexes.

Analyses of the bonding properties in the complexes show strong covalent character of the interaction between ruthenium and *p*-cymene ring. In the binding of arene rings with ruthenium(II) the repulsive Pauli interactions are dominated, however, the electrostatic contribution plays a role and has a stabilizing influence. Moreover, the ΔE_{elstat} is slightly higher than the orbital interaction in the all complexes. On the other hand, when the heteroaromatic ligands are considered as fragments, the electrostatic interaction is the leading stabilization energy except the complex (**4**) in which ΔE_{orb} plays dominant role. It drives the bonding interaction of the occupied MOs of HBO ligand with the *d* orbitals of the ruthenium atom and confirms strong donor properties of HBO ligand. In addition, the ΔE_{Pauli} energies are smaller than that in the *p*-cymene fragments.

The electronic spectra of the complexes were calculated with use of TD-DFT method using the B3LYP functional

Table 5 The electronic transitions for the complex (**2**) calculated with CAM-B3LYP and B3LYP functional by the TD-DFT method

λ (nm)		Contributions	Exp. λ (nm)
CAM-B3LYP	B3LYP		
504.9	503.0	H-2 → LUMO (23%); H-1 → LUMO (45%)	
		H-1 → LUMO (74%)	
458.6	465.1	H-4 → L+1 (23%); H-2 → LUMO (16%); HOMO → L+1 (17%)	458.0
		H-4 → L+1 (10%); H-3 → L+1 (20%); HOMO → L+1 (47%)	
449.2	453.0	H-3 → L+1 (21%); H-3 → LUMO (46%)	
		H-2 → LUMO (42%); H-1 → L+1 (25%)	
384.0	393.7	H-2 → LUMO (12%); H-2 → L+1 (44%)	422.0
		H-2 → LUMO (21%); H-2 → L+1 (30%); H-1 → L+1 (31%)	
375.9	385.5	H-3 → LUMO (12%); H-3 → L+1 (30%); H-1 → L+1 (15%)	
		H-3 → L+1 (20%); H-2 → LUMO (11%); H-2 → L+1 (25%)	
	336.3	H-4 → LUMO (11%); H-3 → LUMO (36%); H-1 → LUMO (20%)	
	327.0	H-4 → L+1 (11%); H-3 → L+1 (33%); HOMO → L+1 (29%)	313.0
	301.4	H-1 → L+2 (28%); HOMO → L+2 (56%)	
	286.8	H-2 → L+2 (28%); HOMO → L+3 (40%)	
261.7	278.8	H-2 → L+2 (17%); H-1 → L+3 (19%); HOMO → LUMO (19%)	277.2
		H-5 → L+1 (48%); H-2 → L+3 (37%)	
257.6	258.5	H-5 → LUMO (20%); H-4 → L+1 (17%); H-1 → L+1 (13%)	
		HOMO → L+4 (85%)	
241.7	248.9	HOMO → L+4 (33%)	
		H-1 → L+4 (61%)	
208.6	216.6	H-8 → LUMO (66%)	
		H-5 → L+3 (94%)	
	214.7	H-12 → LUMO (16%); H-9 → L+1 (36%)	214.2

Fig. 7 The emission spectra of the complexes in the methanolic solutions ($c = 5 \times 10^{-4}$ mol/dm^3) (*Inset* shows a magnified range from 490 to 600 nm)

and its long-range corrected version CAM-B3LYP which uses the Coulomb-attenuating method. The calculations with CAM-B3LYP functional showed worse estimations of excitation energies especially for the transitions with *charge transfer* character.

The emission properties of the complexes were examined. The emissions originating from the lowest energy MLCT state, derived from the excitation involving a $d_\pi \to \pi_{ligand}^*$ transition were observed. This assignment was supported by the analysis of the frontier orbitals of the corresponding complexes, showing a partial contribution from the ligands. In addition, the complicated structure of the luminescence spectra suggest that more than one state is involved in luminescence processes.

Supplementary data

CCDC 808289, CCDC 811596, CCDC 813005, and CCDC 814576 contain the supplementary crystallographic data for complexes [(*p*-cymene)RuCl(BImPhNH)]Cl·(CH$_3$)$_2$CO, [(*p*-cymene)RuCl$_2$(BImNH)], [(*p*-cymene)RuCl$_2$(BTzNH)], and [(*p*-cymene)RuCl(HBO)], respectively. These data can be obtained free of charge from http://www.ccdc.cam.ac.uk/conts/retrieving.html, or from the Cambridge Crystallographic Data Centre, 12 Union Road, Cambridge CB2 1EZ, UK; fax: (+44) 1223-336-033; or e-mail: deposit @ccdc.cam.ac.uk.

References

1. Therrien B (2009) Coord Chem Rev 253:493
2. Therrien B, Süss-Fink G, Govindaswamy P, Saïd-Mohamed C (2007) Polyhedron 26:4065
3. Canivet J, Karmazin-Brelot L, Süss-Fink G (2005) J Organomet Chem 690:3202
4. Hamaker ChG, Halbach DP (2009) Polyhedron 28:2228
5. Kumar Singh A, Kumar P, Yadav M, Shankar Pandey D (2010) J Organomet Chem 695:567
6. Naresh Kumar K, Venkatachalam G, Ramesh R, Liu Y (2008) Polyhedron 27:157
7. Lalrempuia R, Rao Kollipara M (2003) Polyhedron 22:3155
8. Singh A, Chandra M, Sahay AN, Pandey DS, Pandey KK, Mobin SM, Puerta MC, Valerga P (2004) J Organomet Chem 689:1821
9. Gupta G, Prasad KT, Das B, Rao KM (2010) Polyhedron 29:904
10. Chérioux F, Thomas ChM, Monnier T, Süss-Fink G (2003) Polyhedron 22:543
11. Singh A, Singh N, Shankar Pandey D (2002) J Organomet Chem 642:48
12. Lalrempuia R, Rao Kollipara M, Carroll PJ (2003) Polyhedron 22:605
13. Ronconi L, Sadler PJ (2007) Coord Chem Rev 251:1633
14. Süss-Fink G, Khan F-A, Juillerat-Jeanneret L, Dyson PJ, Renfrew AK (2010) J Clust Sci 21:313
15. Das S, Sinha S, Britto R, Somasundaram K, Samuelson AG (2010) J Inorg Biochem 104:93
16. Govender P, Antonels NC, Mattsson J, Renfrew AK, Dyson PJ, Moss JR, Therrien B, Smith GS (2009) J Organomet Chem 694:3470
17. Grgurić-Šipka S, Ivanović I, Rakić G, Todorović N, Gligorijević N, Radulović S, Arion VB, Keppler BK, Tešić ZLj (2010) Eur J Med Chem 45:1051
18. Małecki JG, Jaworska M, Kruszynski R (2007) J Organomet Chem 692:2903
19. Małecki JG, Kruszynski R, Jaworska M, Lodowski P (2007) J Coord Chem 60:741
20. Małecki JG, Kruszynski R, Jaworska M, Lodowski P, Mazurak Z (2008) J Organomet Chem 693:1096
21. Małecki JG (2010) J Coord Chem 63:2268
22. Małecki JG (2010) Trans Met Chem 35:801
23. Małecki JG (2011) J Coord Chem 64:390
24. Frisch MJ, Trucks GW, Schlegel HB, Scuseria GE, Robb MA, Cheeseman JR, Scalmani G, Barone V, Mennucci B, Petersson GA, Nakatsuji H, Caricato M, Li X, Hratchian HP, Izmaylov AF, Bloino J, Zheng G, Sonnenberg JL, Hada M, Ehara M, Toyota K, Fukuda R, Hasegawa J, Ishida M, Nakajima T, Honda Y, Kitao O, Nakai H, Vreven T, Montgomery Jr JA, Peralta JE, Ogliaro F, Bearpark M, Heyd JJ, Brothers E, Kudin KN, Staroverov VN, Kobayashi R, Normand J, Raghavachari K, Rendell A, Burant JC, Iyengar SS, Tomasi J, Cossi M, Rega N, Millam JM, Klene M, Knox JE, Cross JB, Bakken V, Adamo C, Jaramillo J, Gomperts R, Stratmann RE, Yazyev O, Austin AJ, Cammi R, Pomelli C, Ochterski JW, Martin RL, Morokuma K, Zakrzewski VG, Voth GA, Salvador P, Dannenberg JJ, Dapprich S, Daniels AD, Farkas O, Foresman JB, Ortiz JV, Cioslowski J, Fox DJ (2009) Gaussian 09, Revision A.1. Gaussian, Inc., Wallingford
25. Becke AD (1993) J Chem Phys 98:5648
26. Lee C, Yang W, Parr RG (1988) Phys Rev B 37:785
27. Casida ME (1996) In: Seminario JM (ed) Recent developments and applications of modern density functional theory, theoretical and computational chemistry, vol 4. Elsevier, Amsterdam, p 391
28. Yanai T, Tew D, Handy N (2004) Chem Phys Lett 393:51
29. Eichkorn K, Weigend F, Treutler O, Ahlrichs R (1997) Theor Chim Acc 97:119
30. O'Boyle NM, Tenderholt AL, Langner KM (2008) J Comp Chem 29:839
31. Tenderholt AL. QMForge, version 2.1. Stanford University, Stanford
32. Velde GT, Bickelhaupt FM, Baerends EJ, Guerra CF, Van Gisbergen SJA, Snijders JG, Ziegler T (2001) J Comput Chem 22:931
33. Becke AD (1988) Phys Rev A 38:3098
34. Perdew JP, Chevary JA, Vosko SH, Jackson KA, Pederson MR, Singh DJ, Fiolhais C (1992) Phys Rev B 46:6671
35. Dolomanov et al (2009) J Appl Cryst 42:339
36. Sheldrick GM (2008) Acta Cryst A64:112
37. Desiraju GR, Steiner T (1999) The weak hydrogen bond in structural chemistry and biology. Oxford University Press, Oxford
38. Jeffrey GA, Saenger W (1994) Hydrogen bonding in biological structures. Springer, New York